American Mineralogist, Volume 94, pages 1620–1628, 2009

Thermodynamic and crystallographic properties of kornelite [$Fe_2(SO_4)_3 \cdot \sim 7.75H_2O$] and paracoquimbite [$Fe_2(SO_4)_3 \cdot 9H_2O$]

Sonia Ackermann,[1] Biljana Lazic,[2] Thomas Armbruster,[2] Stephen Doyle,[3] Klaus-Dieter Grevel,[1,5] and Juraj Majzlan[1,4,*]

[1]Institute of Mineralogy and Geochemistry, Albert-Ludwigs-University, Albertstrasse 23b, D-79104 Freiburg, Germany
[2]Mineralogische Kristallographie, Institute of Geology, University of Bern, Freiestrasse 3, CH-31012 Bern, Switzerland
[3]Forschungszentrum Karlsruhe, Institute for Synchrotron Radiation, Hermann-von-Helmholtz-Platz 1, D-76344 Eggenstein-Leopoldshafen, Germany
[4]Institute of Geosciences, Friedrich-Schiller University, Burgweg 11, D-07749 Jena, Germany
[5]Institute for Geology, Mineralogy and Geophysics, Ruhr-University Bochum, D-44780 Bochum, Germany

Abstract

Enthalpies of formation of kornelite [$Fe_2(SO_4)_3 \cdot \sim 7.75H_2O$] and paracoquimbite [$Fe_2(SO_4)_3 \cdot 9H_2O$] were measured by acid (5 *N* HCl) solution calorimetry at $T = 298.15$ K. The samples were characterized chemically by an electron microprobe, and structurally by the means of single-crystal, in-house powder, and synchrotron powder X-ray diffraction. The refined structures for the two phases are provided, including estimates of the positions and concentration of non-stoichiometric water in structural channels of kornelite, location of the hydrogen atoms and the hydrogen bonding system in this phase. The measured enthalpies of formation from the elements (crystalline Fe, orthorhombic S, ideal gases O_2 and H_2) at $T = 298.15$ K are –4916.2 ± 4.2 kJ/mol for kornelite and –5295.4 ± 4.2 kJ/mol for paracoquimbite. We have used several algorithms to estimate the standard entropy of the two phases. Afterward, we calculated their Gibbs free energy of formation and constructed a phase diagram for kornelite, paracoquimbite, $Fe_2(SO_4)_3 \cdot 5H_2O$, and $Fe_2(SO_4)_3$ as a function of temperature and relative humidity of air. The topology of the phase diagram is very sensitive to the entropy estimates and the construction of a reliable phase diagram must await better constraints on entropy or Gibbs free energy of formation. Possible remedies of these problems are also discussed.

Keywords: Kornelite, paracoquimbite, thermodynamic properties, enthalpy of formation

Introduction

The minerals kornelite [$Fe_2(SO_4)_3 \cdot \sim 7.75H_2O$] and paracoquimbite [$Fe_2(SO_4)_3 \cdot 9H_2O$] were reported from several localities that are mostly related to former mining sites (Merwin and Posnjak 1937; Nordstrom and Alpers 1999; Joeckel et al. 2005; Qin et al. 2008). The two minerals belong to the group of hydrated Fe(III) sulfates whose other members are lausenite [$Fe_2(SO_4)_3 \cdot 6H_2O$], quenstedtite [$Fe_2(SO_4)_3 \cdot 11H_2O$], and coquimbite [$Fe_2(SO_4)_3 \cdot 9H_2O$]; the latter is the most common mineral within this group. The formation of hydrated iron sulfate minerals is associated with acidic sulfate- and Fe-rich waters that form by the oxidation of common sulfide minerals (pyrite, pyrrhotite, and marcasite) that occur in ores, anoxic soils and sediments, and industrial wastes. The most significant occurrences of such waters are generated in the so-called acid mine drainage (AMD) systems where the acidity and the sulfur and metal content is generated by the oxidation and weathering of ore and gangue minerals (Jambor et al. 2000). In the process of sulfide mineral weathering, considerable amounts of heavy and toxic metals and metalloids can be released into the environment (Jambor et al. 2000). The low pH encountered in these solutions (Nordstrom and Alpers 1999) keeps large quantities of metals and pollutants in aqueous solutions that are, in turn, capable of transporting the pollution over large distances.

The metal and sulfate ions in solution may precipitate to form sulfate minerals, if environmental conditions such as temperature, air humidity, or activities of aqueous ions change. The formation of secondary Fe(III) sulfate minerals exerts control not only over the Fe and sulfate concentration, but also over the concentration of other pollutants. These pollutants may be incorporated into the structure of the Fe(III) sulfates or adsorbed onto their surfaces (Balistrieri et al. 2007).

The thermodynamic properties of Fe(III) sulfate minerals allow estimation of the stability and compute the solubility of these phases in the AMD systems. Additionally, the thermodynamic properties of these minerals are of interest because their presence is inferred on the surface of Mars or confirmed in martian meteorites (Bridges and Grady 2000; Morris et al. 2006; Johnson et al. 2007). A few thermodynamic studies have been carried out on Fe(III) sulfate minerals (Baron and Palmer 2002; Majzlan et al. 2006); consequently, the thermodynamic description of most of them is lacking. Most of the published phase diagrams of Fe(III) sulfate minerals are based on earlier solubility studies and field observations (e.g., Cameron and Robinson 1907; Posnjak and Merwin 1922; Baskerville and Cameron 1935).

* E-mail: Juraj.Majzlan@uni-jena.de

0003-004X/09/1112–1620$05.00/DOI: 10.2138/am.2009.3179

Here we report the formation enthalpy of kornelite and paracoquimbite at the standard temperature and pressure. The kornelite and paracoquimbite samples were synthesized in the laboratory and characterized by an electron microprobe, single-crystal, and powder X-ray diffraction. Using estimates of entropy, we have calculated the stability fields for the $Fe_2(SO_4)_3 \cdot nH_2O$ phases as a function of temperature and relative humidity of the air. The calculated position of the stability fields is very sensitive to the entropy estimates and we show that, without additional constraints on entropy, either direct (measurement of entropy) or indirect (experimental brackets), no reliable phase diagrams can be calculated, even if the experimentally determined formation enthalpies are available.

Materials and methods

The reagents used for the syntheses of the studied phases and the calorimetric solvent were ordered from Alfa Aesar. Sulfuric acid (96% with a density of 1.86 g/cm^3) as well as the ferric sulfate were of analytical grade. The ferric sulfate batch was a fine-grained, pale-brown powder that was X-ray amorphous. MgO crystals were obtained from Alfa Aesar (99.95% on a metal basis) and showed no impurity phases when subjected to an X-ray diffraction (XRD) analysis.

The kornelite sample was synthesized by dissolving 2.5 g of ferric sulfate in 1.17 mL of deionized water. The very viscous yellow solution was transferred into polyethylene flasks, closed and placed into an oven at 75 °C. After 48 h, an initial yellow precipitate, identified as ferricopiapite with XRD analysis, was observed. The sample was left in the oven for an additional 9 days. Afterward, the oven was turned off, the lid of the sample vial removed, and the content of the vial was allowed to cool very slowly to room temperature in the oven. During cooling, the yellow precipitate turned into pale-violet needle-shaped crystals of kornelite.

The paracoquimbite sample was synthesized by dissolving 2.93 g of ferric sulfate in a mixture of 3.1 mL H_2O and 0.526 mL concentrated (96%) sulfuric acid. First, water and sulfuric acid were mixed and allowed to cool to room temperature. Afterward, ferric sulfate was added and dissolved. The viscous yellow suspension transformed into a thick, brown solution after a few minutes. It is important that the ferric sulfate dissolves completely. Any solid particles present shortly after the preparation of the solution are most likely rhomboclase [$(H_5O_2)Fe(SO_4)_2 \cdot 2H_2O$]; this phase will not re-dissolve and was formed because H_2SO_4 was added in excess. The solution was then allowed to slowly age for one year at room temperature and relative humidity of 30–40%. Although the vial remained open throughout the year, little liquid evaporated, most likely because of the low water activity in the concentrated solution. The white powdery mass was then separated from the remaining (but still abundant) mother liquor by filtering and allowed to dry at room temperature.

The kornelite grains were prepared in a form of a standard thin section by polishing with SiC powder and diamond-oil pastes without water. Quantitative electron microprobe data of these grains were obtained with a Cameca SX-100 instrument in the wavelength-dispersive mode using a constant sample current of 4 nA, an accelerating voltage of 15 kV, celestine ($SrSO_4$) as a standard for S, and hematite (Fe_2O_3) for Fe. The counting time on the peaks and background were 10 and 5 s, respectively, for both elements. The short counting times together with the low sample current were necessary to minimize the beam-induced damage of the sample. The beam diameter was 10 µm.

Conventional powder XRD patterns were collected with a Bruker D8 Advance diffractometer, equipped with a Cu$K\alpha$ radiation source, diffracted-beam graphite monochromator, and a scintillation detector. The patterns were collected from 2.0 to 60.0 °2θ, with a step of 0.02 °2θ and dwell of 2 s at each step. All data were processed by Rietveld refinement, with the program GSAS (Larson and Von Dreele 1994), to determine the lattice parameters and to confirm the purity of the samples. Thermal analysis of the samples was carried out with a Perkin Elmer Pyris 1 differential scanning calorimeter (DSC). Approximately 50 mg of the sample was heated in corundum crucibles and in air atmosphere from room temperature to 1200 K with a heating rate of 10 K/min.

Synchrotron powder XRD patterns were collected at the bending magnet beamline PDIFF at the synchrotron light source ANKA in Karlsruhe, Germany. X-rays with wavelengths of 0.7042(1) Å (kornelite) and 1.1824(1) Å (paracoquimbite) were selected with a double Si 111 monochromator. The wavelength and zero of the diffractometer were determined using silicon (NIST standard reference material 640) and quartz as a standard. Each sample was loaded into a glass capillary of 1 mm inner diameter and measured in transmission mode. The intensity of the incoming beam was measured by an ionization chamber and the intensity of the diffracted beam was corrected for the decay of the primary beam. The XRD patterns were collected at room temperature over a range of 2.0 to 40.0 °2θ, with a step size of 0.004 °2θ and a dwell time of 1 s. All data were processed by Rietveld refinement with GSAS (Larson and Von Dreele 1994). The refined parameters were scale factor, lattice parameters, positional parameters, occupancy, and isotropic thermal factors. Lattice parameters, occupancy, and thermal factors of the kornelite sample were compared to the values obtained from the single-crystal XRD experiment (described below). The structure of paracoquimbite was refined from analysis of the synchrotron powder XRD experiment only.

Single-crystal XRD data for kornelite were collected with an APEX II SMART single-crystal diffractometer at the Crystallographic Institute of the University in Bern, Switzerland, employing Mo$K\alpha$ radiation and a graphite monochromator. The data were recorded with a CCD detector. Additional experimental details are summarized in Table 1. The parameters refined for the single-crystal diffraction experiment were positional parameters, occupancy for the interlayer water molecules, and isotropic as well as anisotropic thermal factors.

For the calorimetric experiments, we used a commercial IMC-4400 isothermal microcalorimeter (Calorimetry Sciences Corporation) that we modified for the purposes of acid-solution calorimetry. The liquid bath of the calorimeter was held at a constant temperature of 298.15 K with fluctuations smaller than 0.0005 K. The calorimetric solvent was 25 g of 5 *N* HCl contained in a polyetheretherketone (PEEK) cup with a total volume of 60 mL. The cup was then closed with a PEEK screwable lid and inserted into the calorimeter well. The calorimeter stabilized after ~8 h. During the stabilization and the experiment, the solvent was stirred by a SiO_2 glass stirrer by a motor positioned about 40 cm from the active zone of the instrument. The samples were pressed into pellets and each weighed on a micro-balance with a precision of 0.01 mg (as stated by the manufacturer). The pellets were then dropped through a SiO_2 glass tube into the solvent, and the heat

Table 1. Parameters for X-ray data collection and crystal structure refinement of kornelite

Crystal data	Kornelite
Unit-cell dimensions (Å,°)	a = 14.3125(3) b = 20.1235(5) c = 5.4310(1) β = 96.8133 (14)
Volume (Å^3)	1553.18 (6)
Space group	$P2_1/n$ (no. 14)
Z	4
Chemical formula	$Fe_2(H_2O)_6(SO_4)_3(H_2O)_{1.75}$
μ (mm^{-1})	2.37
Intensity measurement	
Crystal shape	plate
Crystal size (mm)	0.160 × 0.038 × 0.005
Diffractometer	APEX II SMART
X-ray radiation	Mo$K\alpha$, λ = 0.71073 Å
X-ray power	50 kV, 35 mA
Monochromator	graphite
Temperature	293 K
Detector to sample distance	5.95 cm
Measurement method	phi and omega scans
Rotation width	0.5°
Total number of frames	2180
Frame size	512 × 512 pixels
Time per frame	30 s
θ-range for data collection	1.75–24.37
Index ranges	$-16 \le h \le 16$ $-22 \le k \le 23$ $-6 \le l \le 6$
No. of measured reflections	21599
No. of unique reflections	2540
No. of observed reflections [$I > 4\sigma(I)$]	1887
Refinement of the structure	
No. of parameters used in refinement	261
Soft constraints for O-H bonds	0.90(5) Å
R_{int}	0.0750
$R\sigma$	0.0509
$R1$, $I > 4\sigma(I)$	0.0400
$R1$, all data	0.0611
$wR2$ (on F^2)	0.0977
GooF	1.101
$\Delta\rho_{max}$ (eÅ^{-3})	0.86 close to Ow8B
$\Delta\rho_{min}$ (−eÅ^{-3})	−0.53 close to S3

produced or consumed during the dissolution was measured. The heat flow between the reaction cup and the constant temperature reservoir was then integrated to calculate the caloric effect. A typical experiment lasted 120–130 min and the end of the experiment was judged from the return of the baseline to the pre-experiment position. The calorimeter was calibrated by dissolving ~20 mg pellets of KCl in 25 g of deionized water. Prior to each calibration measurement, the potassium chloride was heated overnight in the furnace at 800 K to remove the adsorbed water. The expected heat effect for the calibration runs was calculated from Parker (1965).

Results and discussion

The kornelite crystals are elongated platelets with an average length of around 300 μm (Fig. 1a) and strong polysynthetic twinning, in agreement with the observations of Robinson and Fang (1973). The Fe/S ratio of the synthesized crystals measured by the electron microprobe is 0.62(5) (average of 35 single measurements). Given the experimental difficulties encountered during these measurements, we consider this value to be in a good agreement with the theoretical Fe/S ratio of 0.66.

The paracoquimbite crystals have a well-developed, ditrigonal shape as observed by optical microscopy (Fig. 1b). In crossed nicols, most of the grains shown in Figure 1b appear to be isotropic, i.e., their optical axes are parallel to the microscope axis. This confirms that the dominant form of the crystals is {0001}. The crystals have a diameter of ~25 μm.

The thermogravimetric (TG) and differential thermal (DT) analysis showed that both studied phases decompose in a series of exothermic events (Fig. 2). Kornelite dehydrates in one step, whereas there are two dehydration steps for paracoquimbite. Maximum heat flow for the dehydration of kornelite was recorded at 477 K, and for the dehydration of paracoquimbite at 427 and 514 K. The final event centered at 1012 K for both sulfates is the loss of SO_2. The TG curves can be used to determine the water content of the studied sulfates. The dehydration events are followed, in each case, by a gently sloping plateau, and it is difficult to determine the point that represents the complete loss of structural water. For kornelite, the center of the plateau gives the value of n in $Fe_2(SO_4)_3 \cdot nH_2O$ of 7.47, whereas the high-temperature margin of the plateau gives n = 7.98. For paracoquimbite, the value of n in the center of the plateau is

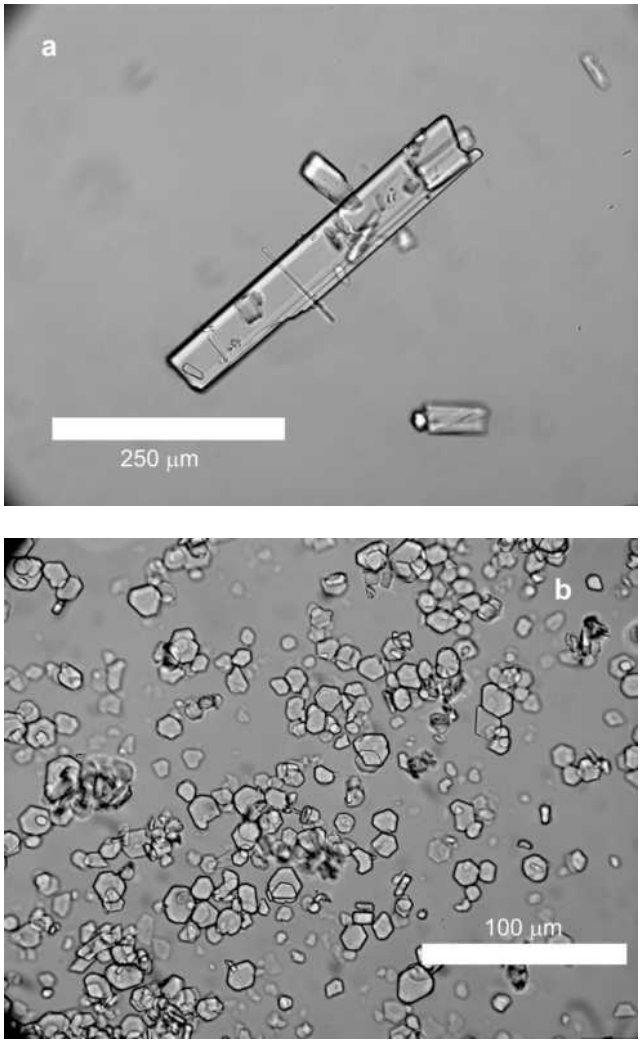

Figure 1. Optical light microscopy images of kornelite (**a**) and paracoquimbite (**b**) crystals used for the thermodynamic measurements.

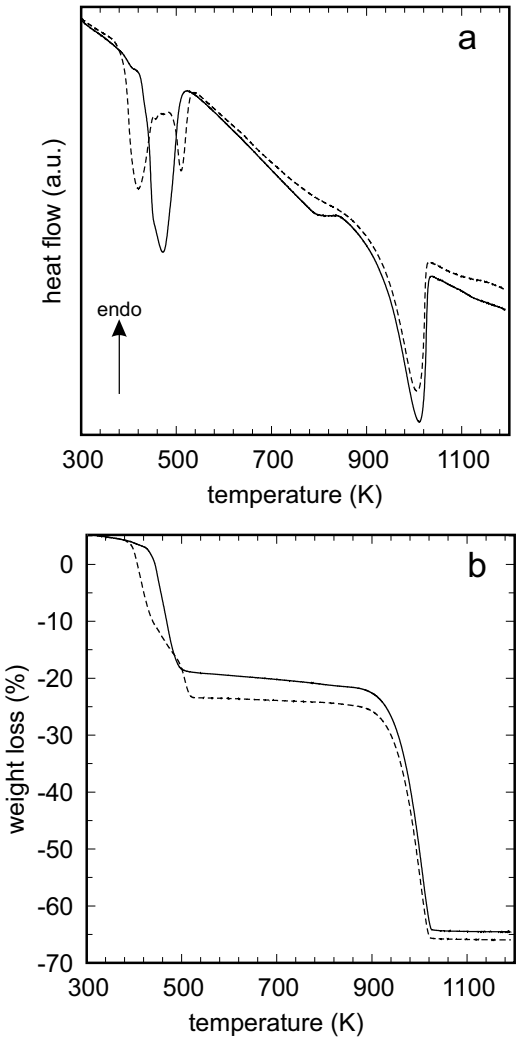

Figure 2. Results of differential thermal (**a**) and thermogravimetric (**b**) analysis of the two studied sulfates. The data for kornelite are shown by the solid curve, and those for paracoquimbite are shown by the dashed curve.

9.02, and the value at the high-temperature margin is $n = 9.38$. Because of these uncertainties, we determined the water content from the refined X-ray diffraction structures and used this water content for the thermodynamic analysis.

Refined crystal structure of kornelite

The monoclinic structure of kornelite was first solved by Robinson and Fang (1973) and is composed of corrugated sheets of corner-sharing SO_4 tetrahedra and $Fe(O,OH_2)_6$ octahedra (Fig. 3). Actually, 6 H_2O molecules per formula unit (pfu) are part of the Fe^{3+} coordination. All hydrogen positions of these H_2O molecules could be extracted from difference-Fourier maps and subsequently refined with a fixed isotropic displacement parameter of $U_{iso} = 0.05$ Å^3. The corrugated sheets parallel to (100) are stacked along the *a* axis. The narrow gaps between the sheets are linked by hydrogen bonds (Fig. 3) thus, at the wider layer spacing, endless channel-like openings are formed parallel to [001]. This empty space is occupied by stacks of additional H_2O molecules accepting hydrogen bonds from H_2O molecules of the Fe^{3+} coordination. The periodicity along *c* is 5.43 Å. Thus, if 2 H_2O molecules were stacked along *c*, they would be separated by ca. 2.7 Å, which is shorter than the O···O distance in most ice modifications and in the ice-like chains (O···O: 2.93 Å) in the channels of the zeolite bikitaite (Quartieri et al. 1999). We have modeled the channel-like H_2O in kornelite (1) by two partially occupied H_2O sites with anisotropic displacement parameters leading to 1.71(5) H_2O pfu strongly smeared parallel to [001] (Fig. 4). In a second model, (2) we have simulated the channel occupants by four partly occupied H_2O sites with a common isotropic displacement parameter. In this approach, the channel-like H_2O occupancies summed up to 1.75(5) H_2O pfu supporting the H_2O concentration obtained by the previous model. Both models indicate an average O(H_2O) to O(H_2O) distance of 3.16 Å, which is considerably longer than corresponding distances for H_2O chains in the channel of bikitaite (Quartieri et al. 1999). Thus the H_2O-H_2O interaction parallel to the channels is assumed to be very weak.

There are two possible ways in which H_2O could be arranged within the channels: (1) in a disordered fashion as modeled for the structure refinement presented here, and (2) in a periodic way, but the periodicity of the channel-like H_2O molecules is incommensurate with the 5.43 Å periodicity of the corrugated sheet (in the *c* direction). In the latter case, very weak satellite reflections should occur in the single-crystal X-ray pattern. However, due to the small crystal size and the minor contribution of ca. 1.75(5) H_2O molecules (ca. 5 wt%) relative to the remaining structural building blocks of $Fe_2(H_2O)_6(SO_4)_3$ composition, these satellites will be too weak to be detected. Thus, on the basis of the present data, incommensurate and disordered channel H_2O arrangement cannot be distinguished. The S-O and Fe-O distances calculated from our data (see supplementary table[1]) correspond well to those published by Robinson and Fang (1973).

Kornelite is a phase with a variable hydration state (Hasenmueller and Bish 2005). The major goal of the structural characterization of kornelite was to understand and to reliably estimate the nonstoichiomteric H_2O concentration in the structural channels. As a byproduct of this approach, a strongly improved structural model including the hydrogen bonding system in synthetic kornelite could be developed (Tables 2 and 3).

The refined lattice parameters from our single-crystal diffraction experiment (Table 1) agree well with those published by Rob-

[1] Deposit item AM-09-052, Supplementary Table and CIF. Deposit items are available two ways: For a paper copy contact the Business Office of the Mineralogical Society of America (see inside front cover of recent issue) for price information. For an electronic copy visit the MSA web site at http://www.minsocam.org, go to the American Mineralogist Contents, find the table of contents for the specific volume/issue wanted, and then click on the deposit link there.

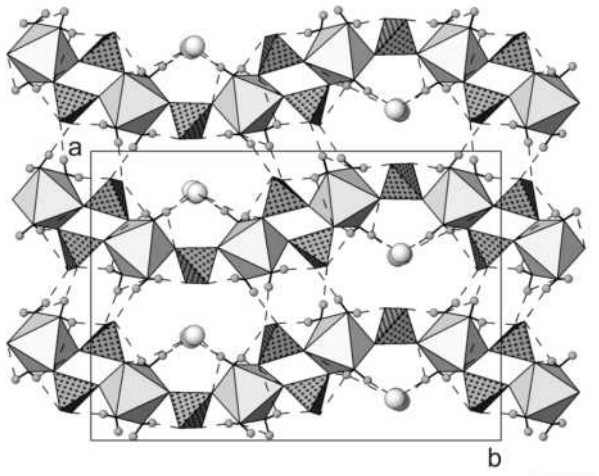

FIGURE 3. A polyhedral drawing of the kornelite structure projected parallel to *c*. Corrugated sheets (seen edge-wise) are formed by corner-sharing SO_4 tetrahedra and $Fe^{3+}(O,H_2O)$ octahedra. Protons (H) are represented by small spheres. Dashed lines indicate hydrogen bonds. Channel H_2O is shown by large spheres accepting hydrogen bonds from H_2O-coordinating Fe^{3+}.

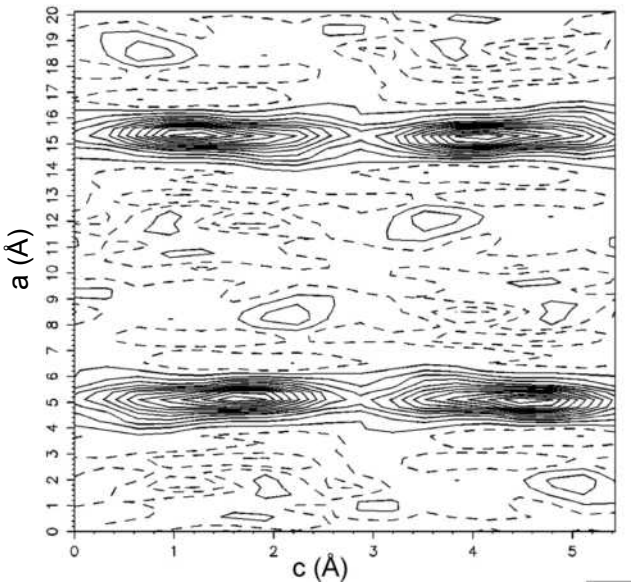

FIGURE 4. A difference Fourier electron-density map of kornelite after removing channel H_2O from the atom list. Channel H_2O is smeared out parallel to the *c*-axis and displays two elongate thickenings. Solid lines represent 0.5 e/Å^3 contours, whereas dashed lines represent –0.5 e/Å^3.

TABLE 2. Atomic coordinates and isotropic displacement parameters for kornelite

Atom	*x*	*y*	*z*	U_{eq}/U_{iso}
Fe1	0.83024(5)	0.10292(3)	0.29736(12)	0.0177(2)
Fe2	0.83302(5)	0.38536(3)	0.77282(12)	0.0170(2)
S1	0.64829(9)	0.03559(6)	0.4920(2)	0.0168(3)
S2	0.89887(9)	0.24297(6)	0.5567(2)	0.0180(3)
S3	0.84574(9)	–0.04884(6)	0.0716(2)	0.0169(3)
O1	0.5879(2)	0.05702(17)	0.6719(6)	0.0274(9)
O2	0.7297(2)	0.08181(17)	0.5036(6)	0.0258(9)
O3	0.6894(3)	–0.03050(17)	0.5565(6)	0.0299(9)
O4	0.6000(2)	0.03345(18)	0.2411(6)	0.0285(9)
O5	0.9554(2)	0.26888(17)	0.3733(6)	0.0289(9)
O6	0.8358(2)	0.29533(16)	0.6342(6)	0.0255(9)
O7	0.9580(2)	0.21632(18)	–0.2315(6)	0.0327(9)
O8	0.8330(2)	0.19135(17)	0.4446(6)	0.0287(9)
O9	0.9048(2)	–0.04728(17)	–0.1283(6)	0.0278(9)
O10	0.8954(2)	–0.07560(17)	0.3002(6)	0.0250(9)
O11	0.8099(2)	0.01883(16)	0.1094(6)	0.0275(9)
O12	0.7622(2)	–0.09166(17)	0.0074(6)	0.0263(9)
OW1	0.9422(3)	0.36298(19)	1.0248(7)	0.0302(10)
OW2	0.5729(3)	–0.07599(18)	–0.0664(6)	0.0224(8)
OW3	0.7619(3)	–0.15293(19)	0.5259(8)	0.0378(11)
OW4	0.7457(3)	0.1413(2)	0.0150(8)	0.0458(12)
OW5	0.9206(3)	0.06040(18)	0.5604(6)	0.0253(9)
OW6	0.9437(3)	0.1251(2)	0.1302(7)	0.0320(11)
OW7A*	0.8529(8)	–0.2552(5)	1.203(3)	$0.064(3)^{iso}$
OW7B†	0.8614(16)	–0.2523(11)	1.072(6)	$0.064(3)^{iso}$
OW8A‡	0.8638(9)	–0.2473(6)	0.837(3)	$0.064(3)^{iso}$
OW8B§	0.8565(5)	–0.2589(4)	0.6628(16)	$0.064(3)^{iso}$
H1A	0.941(4)	0.334(2)	1.132(9)	0.050^{iso}
H1B	0.981(4)	0.393(3)	1.067(10)	0.050^{iso}
H2A	0.515(3)	–0.065(3)	–0.137(10)	0.050^{iso}
H2B	0.593(4)	–0.044(2)	0.025(9)	0.050^{iso}
H3A	0.795(4)	–0.126(3)	0.485(11)	0.050^{iso}
H3B	0.792(4)	–0.187(2)	0.546(11)	0.050^{iso}
H4A	0.717(4)	0.114(3)	–0.067(10)	0.050^{iso}
H4B	0.708(4)	0.174(3)	0.036(11)	0.050^{iso}
H5A	0.908(4)	0.027(2)	0.647(9)	0.050^{iso}
H5B	0.980(2)	0.068(3)	0.606(10)	0.050^{iso}
H6A	0.939(5)	0.149(3)	0.042(12)	0.050^{iso}
H6B	0.988(4)	0.102(3)	0.126(11)	0.050^{iso}

* Occupancies of channel H_2O: 0.46(2).
† Occupancies of channel H_2O: 0.24(2).
‡ Occupancies of channel H_2O: 0.40(1).
§ Occupancies of channel H_2O: 0.66(1).

inson and Fang (1973). Recalculating the occupancies of O atoms that belong to the channel H_2O results in 1.75(5) H_2O molecules per formula unit (pfu), which is in fair agreement, considering the humidity dependence, with 1.55(2) pfu channel H_2O refined from our synchrotron powder X-ray diffraction experiment (Table 4). Both values are considerably higher than the occupancy (1.25 H_2O pfu) reported by Robinson and Fang (1973).

Refined crystal structure of paracoquimbite

The trigonal crystal structures of paracoquimbite and coquimbite are polytypic. They are both composed of polyhedral clusters of $Fe(O,OH_2)_6$ octahedra and SO_4 tetrahedra, isolated $Fe(H_2O)_6$ octahedra, and H_2O molecules (Robinson and Fang 1971). These structural fragments form slabs that are stacked along the *c* axis and are mutually interconnected solely by hydrogen bonds. The positions of hydrogen atoms in either the coquimbite or the paracoquimbite structure have not been determined experimentally. Positions of hydrogen atoms are known only for the structure of $Fe_2(SeO_4)_3 \cdot 9H_2O$, which is isostructural with coquimbite (Giester and Miletich 1995). Using their structural model for $Fe_2(SeO_4)_3 \cdot 9H_2O$, we identified the O atoms that form H_2O molecules in the paracoquimbite structure. The refinement of the occupancy of these O atoms confirmed the water content of 9 H_2O molecules per formula unit (Table 4).

Thermodynamic measurements

The measured dissolution enthalpy of a phase in a suitably chosen medium can be used to calculate its enthalpy of formation. To this end, the dissolution enthalpies of a set of reference compounds in the same medium must be also determined, since enthalpy has no absolute scale. From the dissolution enthalpies and the formation enthalpies of the reference compounds, the enthalpy of formation of the phase of interest can be calculated via a thermochemical cycle, using Hess's law. This law states that the heat evolved or absorbed in a chemical process is the same whether the process takes place in one or in several steps.

Our reference compounds were α-$MgSO_4$, MgO (periclase), and γ-FeOOH (lepidocrocite). Their thermodynamic properties are well known (DeKock 1986; Robie and Hemingway 1995; Majzlan et al. 2006). The dissolution enthalpy of H_2O (i.e., enthalpy of dilution of the acid) was tabulated over a range of HCl concentrations by van Nyus (1943) and Parker (1965) and was calculated from these sources. The dissolution reactions of the reference compounds are reported in Table 5 (reactions 1–4).

Thermodynamic properties of kornelite and paracoquimbite

The dissolution enthalpies of kornelite and paracoquimbite were measured, and the enthalpy of formation was calculated via a thermochemical cycle (Table 5) using the dissolution enthalpies (reactions 1–5 in Tables 5 and 6) and the enthalpies of formation of α-$MgSO_4$, γ-FeOOH, H_2O, and MgO (reactions 7–10). The pellet weight for all phases used in calorimetry was calculated on the basis of stoichiometry with 3 mg MgO according to Equation 6 in Table 5. The pellet mass was monitored during the calorimetric experiments to arrive at an identical final molality for all aqueous species in our experiments. The resulting enthalpies of formation from the elements at $T = 298.15$ K are –4916.2 ± 4.2 kJ/mol for kornelite and –5295.4 ± 4.2 kJ/mol for paracoquimbite.

TABLE 3. Anisotropic displacement parameters U_{ij} of kornelite

Atom	U_{11}	U_{22}	U_{33}	U_{23}	U_{13}	U_{12}
Fe1	0.0192(5)	0.0140(4)	0.0196(4)	–0.0014(3)	0.0017(3)	0.0007(3)
Fe2	0.0182(5)	0.0142(4)	0.0182(4)	–0.0006(3)	0.0008(3)	–0.0009(3)
S1	0.0176(7)	0.0143(7)	0.0183(6)	0.0014(5)	0.0021(5)	0.0013(6)
S2	0.0192(8)	0.0125(7)	0.0223(6)	0.0003(5)	0.0028(5)	–0.0003(6)
S3	0.0162(7)	0.0164(7)	0.0176(6)	–0.0001(5)	0.0007(5)	0.0004(6)
O1	0.028(2)	0.032(2)	0.0240(18)	0.0044(16)	0.0112(16)	0.0123(18)
O2	0.024(2)	0.022(2)	0.032(2)	–0.0035(15)	0.0059(16)	–0.0122(17)
O3	0.038(2)	0.022(2)	0.032(2)	0.0115(16)	0.0159(17)	0.0096(18)
O4	0.025(2)	0.036(2)	0.0221(19)	–0.0088(16)	–0.0075(16)	0.0054(18)
O5	0.031(2)	0.027(2)	0.031(2)	0.0091(16)	0.0126(17)	–0.0010(18)
O6	0.022(2)	0.015(2)	0.040(2)	–0.0109(16)	0.0074(16)	0.0005(16)
O7	0.031(2)	0.032(2)	0.033(2)	0.0121(17)	–0.0056(17)	0.0051(19)
O8	0.021(2)	0.020(2)	0.046(2)	–0.0152(17)	0.0069(17)	–0.0045(17)
O9	0.023(2)	0.035(2)	0.0278(19)	0.0107(16)	0.0110(16)	0.0073(18)
O10	0.021(2)	0.030(2)	0.0225(18)	0.0074(15)	–0.0034(15)	0.0000(17)
O11	0.033(2)	0.019(2)	0.0291(19)	–0.0063(16)	–0.0030(16)	0.0066(17)
O12	0.021(2)	0.030(2)	0.0260(19)	0.0008(16)	–0.0042(16)	–0.0131(17)
OW1	0.031(3)	0.030(3)	0.028(2)	0.0099(17)	–0.0055(18)	–0.0099(19)
OW2	0.019(2)	0.024(2)	0.024(2)	–0.0078(15)	0.0013(16)	0.0032(18)
OW3	0.048(3)	0.017(2)	0.054(3)	0.007(2)	0.033(2)	0.006(2)
OW4	0.060(3)	0.027(3)	0.044(3)	–0.002(2)	–0.024(2)	0.007(2)
OW5	0.021(2)	0.025(2)	0.028(2)	0.0106(16)	–0.0030(17)	–0.0024(19)
OW6	0.035(3)	0.026(3)	0.038(2)	0.0122(18)	0.016(2)	0.010(2)

The hydration state of kornelite must be known and taken into account when conducting the calorimetric experiments to calculate the correct pellet mass and the corresponding molecular mass of the sample. We have adopted the hydration state determined from the single-crystal X-ray diffraction experiments for two reasons. First, for the calorimetric experiments, the kornelite crystals were quickly ground, pressed into a pellet, and dropped into the calorimeter, the whole procedure lasting <10 min. Therefore, the hydration state of the single crystals is more representative for the calorimetric sample than that of the powder exposed to the ambient air for several hours during the powder XRD measurements. Second, the precision of the occupancy determination is better for the single-crystal work, although we acknowledge that this does not necessarily equate to better accuracy.

TABLE 4. Parameters for powder X-ray data collection and crystal-structure refinement of the kornelite and paracoquimbite samples

	Kornelite	Paracoquimbite
Chemical formula	$Fe_2(H_2O)_6(SO_4)_3 \cdot 1.55(2)H_2O$	$Fe_2(SO_4)_3 \cdot 9H_2O$
Lattice parameters (Å, °)	a = 14.3184(1), b = 20.133(1) c = 5.4325(1), β = 96.813(1)	a = 10.9658(1), c = 51.468(5)
Unit-cell volume (Å^3)	1566.07	5359.86
Space group	$P2_1/n$	$R\bar{3}$
Z	4	12
Refined parameters	148	98
Wavelength (Å)	0.7042(1)	1.1824(1)
2θ range	2.9–40.0	2.9–40.0
wR_p	0.1998	0.0591
R_p	0.1522	0.0474
χ^2	1.91	4.28

TABLE 5. Thermochemical cycle for kornelite and paracoquimbite

Reaction number and reaction
1 α-$MgSO_4$ (cr) = Mg^{2+} (aq) + SO_4^{2-} (aq)
2 γ-FeOOH (cr) + $3H^+$ (aq) = Fe^{3+} (aq) + $2H_2O$ (aq)
3 H_2O (l) = H_2O (aq)
4 MgO (cr) + $2H^+$ (aq) = Mg^{2+} (aq) + H_2O (aq)
5 $Fe_2(SO_4)_3(H_2O)_n$ (cr) = $2Fe^{3+}$ (aq) + $3SO_4^{2-}$ (aq) + nH_2O (aq)
6 3α-$MgSO_4$ (cr) + 2γ-FeOOH (cr) + $(n-1)H_2O$ (l) = 3MgO (cr) + $Fe_2(SO_4)_3 \cdot nH_2O$ (cr)
7 Mg (cr) + S (cr) + $2O_2$ (g) = α-$MgSO_4$ (cr)
8 Fe (cr) + O_2 (g) + ½H_2 (g) = γ-FeOOH (cr)
9 H_2 (g) + ½O_2 (g) = H_2O (l)
10 Mg (cr) + ½O_2 (g) = MgO (cr)
11 2Fe (cr) + 3S (cr) + $[6+(n/2)]O_2$ (g) + nH_2 (g) = $Fe_2(SO_4)_3 \cdot nH_2O$ (cr)

Notes: Abbreviations: cr = crystalline; l = liquid; aq = aqueous species; g = gas. n = 7.75 (kornelite); n = 9 (paracoquimbite). All reactants and products are at T = 298.15 K.

TABLE 6. Measured and calculated enthalpies (in kJ/mol); reactions are given in Table 5

Reaction enthalpy	
$\Delta H_1 = \Delta H_{dissolution(\alpha\text{-}MgSO_4)} = -53.50^* \pm 0.48^\dagger$ (7)‡	Majzlan et al. (2006)
$\Delta H_2 = \Delta H_{dissolution(\gamma\text{-}FeOOH)} = -46.15 \pm 0.23$(10)	Majzlan et al. (2006)
$\Delta H_3 = \Delta H_{dilution} = -0.54$	calculated from Parker (1965)
$\Delta H_4 = \Delta H_{dissolution(MgO)} = -149.68 \pm 0.60$(9)	Majzlan et al. (2006)
$\Delta H_{5K} = \Delta H_{dissolution(kornelite)} = +19.12 \pm 0.20$(5)	
$\Delta H_{5P} = \Delta H_{dissolution(paracoquimbite)} = +40.41 \pm 0.63$(3)	
$\Delta H_{6K} = 3\Delta H_1 + 2\Delta H_2 + 6.53\Delta H_3 - 3\Delta H_4 - \Delta H_{5K} = 173.4 \pm 2.4$	
$\Delta H_{6P} = 3\Delta H_1 + 2\Delta H_2 + 8\Delta H_3 - 3\Delta H_4 - \Delta H_{5P} = 154.1 \pm 2.4$	
$\Delta H_7 = \Delta H_{formation(\alpha\text{-}MgSO_4)} = -1288.8 \pm 0.5$	DeKock (1986)
$\Delta H_8 = \Delta H_{formation(\gamma\text{-}FeOOH)} = -549.4 \pm 1.4$	Majzlan et al. (2003)
$\Delta H_9 = \Delta H_{formation(water)} = -285.8 \pm 0.1$	Robie and Hemingway (1995)
$\Delta H_{10} = \Delta H_{formation(MgO)} = -601.6 \pm 0.3$	Robie and Hemingway (1995)
$\Delta H_{11K} = \Delta H_6 + 3\Delta H_7 + 2\Delta H_8 + 6.75\Delta H_9 - 3\Delta H_{10} = -4916.2 \pm 4.2$§	
$\Delta H_{11P} = \Delta H_6 + 3\Delta H_7 + 2\Delta H_8 + 8\Delta H_9 - 3\Delta H_{10} = -5295.4 \pm 4.2$§	

* Mean.
† Two standard deviations of the mean.
‡ Number of measurements.
§ Error propagated as described by Taylor (1982).

The dissolution enthalpies of the hydrated ferric sulfates become more endothermic with increasing water content (Fig. 5). This trend is expected as the hydration process for the less hydrated phases is energetically more favorable. This observation also served as a qualitative evidence of the correctness of our calorimetric results. A linear fit to the dissolution enthalpies (Fig. 5) could be used to derive the formation enthalpies of other $Fe_2(SO_4)_3 \cdot nH_2O$ compounds, for example, $Fe_2(SO_4)_3 \cdot 7H_2O$, if such a value should be needed.

The uncertainties of the measured data are reported as two standard deviations of the mean and are propagated by a standard procedure (Taylor 1982). The calculated enthalpy change ΔH_{calc} is a function of measured enthalpies ΔH_1, ΔH_2, ΔH_3, ... ΔH_m, such that $\Delta H_{calc} = \nu_1\Delta H_1 + \nu_2\Delta H_2 + \nu_3\Delta H_3 + ... + \nu_m\Delta H_m$, where ν_1, ν_2, ν_3, ... ν_m are the stoichiometric coefficients.

Entropy. Beside the formation enthalpy, the calculation of the Gibbs free energy also requires the knowledge of the standard entropy, $S°$. The standard entropy (entropy at T = 298.15 K and $P = 10^5$ Pa) of a phase can be estimated by assuming that the entropy change of a suitably defined reaction is zero. Such reaction must: (1) involve the phase whose entropy is to be estimated; (2) involve only solid crystalline phases; and (3) include similar or identical coordination of the elements in all compounds (see Latimer 1952; Holland 1989). In our case, such reaction is:

$$Fe_2(SO_4)_3 + n\,Mg(OH)_2 = Fe_2(SO_4)_3 \cdot nH_2O + n\,MgO \qquad (12)$$

where n = 7.75 for kornelite and n = 9 for paracoquimbite. The entropy change of reaction 12 is:

$$\Delta S_{12} = 0 = nS°(MgO) + S°[Fe_2(SO_4)_3 \cdot nH_2O] - nS°[Mg(OH)_2] - S°[Fe_2(SO_4)_3].$$

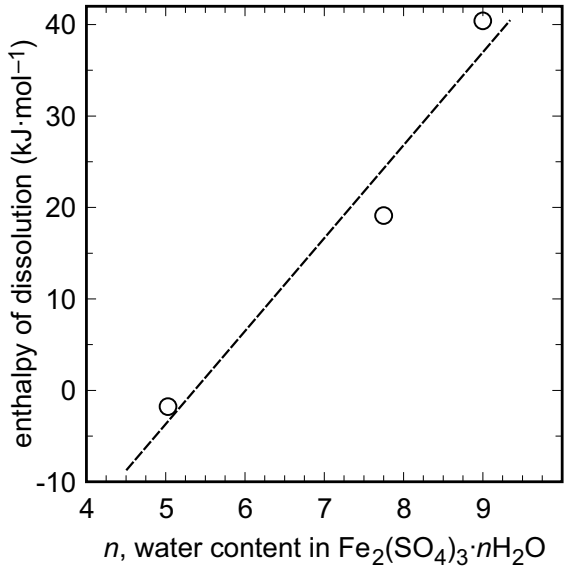

FIGURE 5. Dissolution enthalpies of selected Fe(III) sulfates in 5 N HCl in dependence of the number of water molecules in their structure. The experimental errors (see Table 6) are smaller than the symbol size.

The magnetic contribution to the entropy is accounted for by including $Fe_2(SO_4)_3$ in reaction 12. This is true because the temperature for which reaction 12 is considered is $T = 298.15$ K, whereas the Néel (magnetic) transition for $Fe_2(SO_4)_3$ occurs at $T_N = 30.0$ K (Majzlan et al. 2005). In that case, when $T_N << T$, the magnetic heat capacity at T is negligible and the entire magnetic entropy well accounted for below T.

The entropy contribution accounting for the H_2O content in the crystal structure was calculated by using MgO and $Mg(OH)_2$ because Mg in both cases has the same coordination and cancels out during the calculations. The resulting estimates are listed in Table 7. This approach may lead to an underestimation of the entropy because both kornelite and paracoquimbite contain free H_2O molecules in their structures. The contributions of these molecules to the overall vibrational entropy is probably larger than that of the tightly bound OH groups in the structure of $Mg(OH)_2$. Kornelite may have an additional configurational entropy term resulting from the disorder of the H_2O molecules in its structure, as shown by our single-crystal diffraction study (Fig. 4). Interestingly, even paracoquimbite, where all sites are fully occupied, may possess configurational entropy. The sixfold rings of H_2O molecules in the structure of paracoquimbite could have two possible orientations of hydrogen bonds, which would result in additional entropy. A similar case for configurational entropy in $Na_2SO_4 \cdot 10H_2O$ was documented by Pitzer and Coulter (1938) and Ruben et al. (1961).

Table 7. Components used in the estimation of entropy and their values and the estimated entropy for kornelite and paracoquimbite

Component	$S°$ [J/(mol·K)]	
MgO	26.9 ± 0.2	Robie and Hemingway (1995)
$Mg(OH)_2$	63.2 ± 0.1	Robie and Hemingway (1995)
$Fe_2(SO_4)_3$	305.6 ± 0.6	Majzlan et al. (2005)
kornelite	586.9 ± 2.5	this work
paracoquimbite	632.3 ± 2.9	this work

The stability of Fe(III) sulfates

The Fe(III) sulfate minerals form from aqueous solution with a high concentration of H^+, metals, and sulfate ions. Once crystallized, they may transform to other Fe(III) sulfates depending on the temperature and the relative humidity (RH) of the air. Using our data, we should be able to calculate phase diagrams for the Fe(III) sulfates and compare these phase diagrams with observations from nature or experiment. The equilibria calculations that involve very concentrated aqueous solutions are difficult because the ion activities cannot be derived from simple equations such as the Debye-Hückel equation. On the other hand, the calculations that involve water vapor in the air are easier because the properties of water vapor are well known. Therefore, we attempted to outline the stability fields for anhydrous $Fe_2(SO_4)_3$ (data from Majzlan et al. 2005), $Fe_2(SO_4)_3 \cdot 5H_2O$ (Majzlan et al. 2006), kornelite, and paracoquimbite (this study) as a function of temperature and RH. Figure 6a shows that, when using the measured formation enthalpies and estimated entropies (Tables 6 and 7, respectively), we arrive at an impossible topology of the phase diagram. Kornelite is predicted to exist both in the high- and low-temperature region of the diagram, and the $Fe_2(SO_4)_3 \cdot 5H_2O$ and paracoquimbite have a stability field in between.

It is reasonable to assume that our measured $\Delta H_f°$ values are not the cause of the anomalous results in Figure 6a. Using acid-solution calorimetry and identical reference compounds as in this work, we have previously measured the $\Delta H_f°$ for monoclinic $Fe_2(SO_4)_3$ (Majzlan et al. 2005) and found that the value agrees very well with previous determinations from a variety of sources and methods.

The entropy values, being only estimates, are the numbers to be examined more closely. As an example, consider kornelite, whose estimated entropy here is 586.9 J/(mol·K) (Table 7). Hemingway et al. (2002) used a different algorithm to estimate the entropy of ferric sulfate hydrates. They assumed that each H_2O molecule adds 39.75 J/(mol·K) of entropy. Using their algorithm and the values in their Table 2, the $S°$ for kornelite with composition $Fe_2(SO_4)_3 \cdot 7.75H_2O$ would be 620.4 J/(mol·K). The difference between these two values, 33.5 J/(mol·K), accounts for 10.0 kJ/mol difference in the Gibbs free energy of formation at $T = 298.15$ K. This is a large discrepancy and it can be expected that this difference will have a substantial impact on the phase diagram. A similar difference can be found between two different entropy estimates for paracoquimbite. Therefore, we have tested different entropy values for the studied ferric sulfates. As discussed above, beside the vibrational entropy, both of these phases may have additional configurational entropy, and the "true" entropy of these phases is likely higher than the estimates. Setting the $S°$(kornelite) to 635 J/(mol·K) and $S°$(paracoquimbite) to 660 J/(mol·K), another phase diagram can be calculated (Fig. 6b). The $S°$(kornelite) value was chosen to satisfy two experimental observations (see below). The $S°$(paracoquimbite) value was simply chosen to position the kornelite-paracoquimbite univariant curve into the correct portion of the phase diagram, recognizing that, in the absence of experimental data, no firm constraints exist on the location of the curve. The topology of this diagram is realistic and it also satisfies the experimental observation on the stability of the Fe(III) sulfates reported by Chipera et al. (2007) (shown by a circle in Fig. 6b). They observed that an amorphous hydrated ferric sulfate converts to pure kornelite when exposed to air with RH of 43% at $T = 348$ K. The diagram also satisfies our observation that $Fe_2(SO_4)_3 \cdot 5H_2O$ (shown by a diamond in Fig. 6b) is produced if an amorphous ferric sulfate is allowed to equilibrate at 332 K and RH of 29%. However, in this case, an additional phase was also present and the consequences of this are discussed below.

The purpose of this exercise is not to prove that these entropy estimates are correct. The purpose is to document that the measured formation enthalpies, together with reasonable estimates of entropies, are able to produce a correct phase diagram. The entropy values, however, need to be constrained much better to arrive at a reliable thermodynamic data set for the ferric sulfate minerals. The problem of missing reliable entropies could be mediated in several ways.

(1) Direct measurement of entropy for the ferric sulfates. We have already re-measured the heat capacity and entropy of the anhydrous monoclinic $Fe_2(SO_4)_3$ (Majzlan et al. 2005) because the earlier measurement (Pankratz and Weller 1969) neglected the significant contribution of magnetic heat capacity. The hydrated ferric sulfates are difficult to measure because they will likely dehydrate in the vacuum chambers of the adiabatic

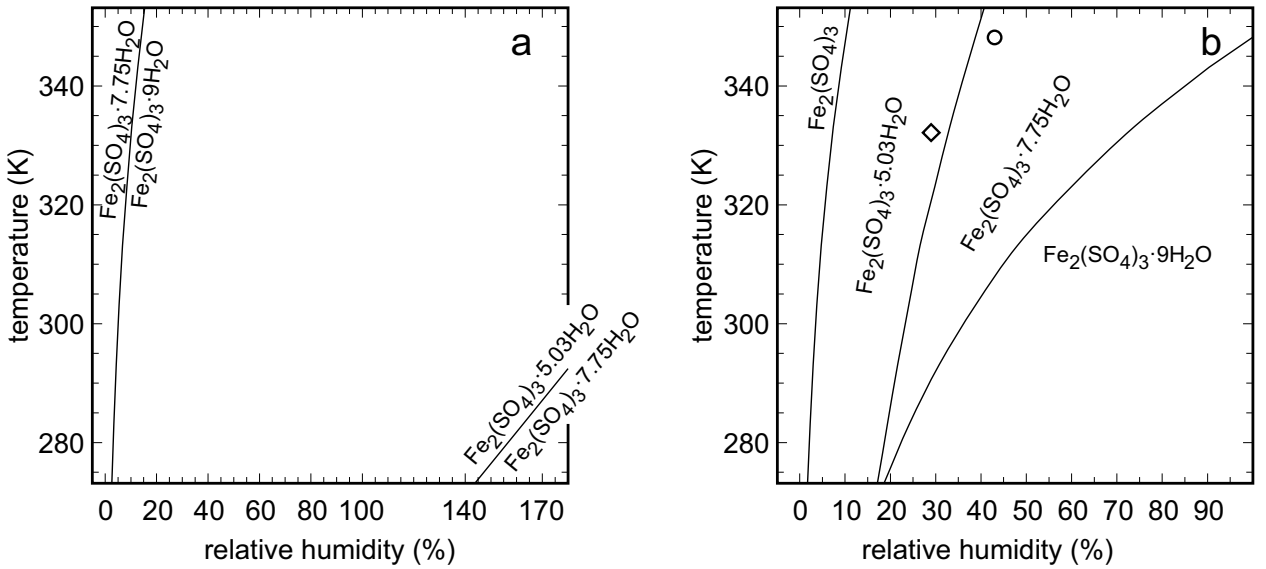

FIGURE 6. (**a**) A phase diagram calculated with the measured enthalpies of formation (this work and Majzlan et al. 2006) and estimated entropies (see Table 7 in this work and Table 14 in Majzlan et al. 2006). This diagram shows an impossible relationship for the stability of the three ferric sulfates. To display the equilibrium between kornelite and $Fe_2(SO_4)_3 \cdot 5.03H_2O$, unrealistic relative humidities higher than 100% had to be plotted on the abscissa. (**b**) A phase diagram calculated with the same data as in **a** with the exception of $S°$(kornelite) and $S°$(paracoquimbite) (see text for details). The data for $Fe_2(SO_4)_3$ (all experimentally measured) are from Majzlan et al. (2005). The circle is the experimental observation of Chipera et al. (2007) who found that kornelite is the phase stable at T = 348 K and RH of 43%. The diamond shows our result that $Fe_2(SO_4)_3 \cdot 5H_2O$ and rhomboclase crystallized from a starting amorphous ferric sulfate at 332 K and RH of 29%.

calorimeters. New advances in this field (Marriott et al. 2006), however, seem to be promising and may yield reliable values even for the hydrated phases.

(2) Combination of temperature-RH brackets with the measured enthalpies of formation. The formation enthalpies presented in this paper and in Majzlan et al. (2006), together with reasonable estimates of entropies, could be refined if reliable temperature-RH brackets are available. As noted by Chipera et al. (2007), experiments that could establish such brackets are plagued by sluggishness and disequilibrium. We have also attempted to carry out a set of such experiments and found that in addition to an $Fe_2(SO_4)_3 \cdot nH_2O$ phase, rhomboclase [$(H_5O_2)Fe(SO_4)_2 \cdot 2H_2O$] is always present. In our experiments, just like in those of Chipera et al. (2007), we have used an amorphous hydrated $Fe_2(SO_4)_3$ as a starting chemical. The formation of rhomboclase from this chemical, means that the sample consists of a crystalline solid (rhomboclase) and a residual iron-rich liquid. In that case, the most likely control over which $Fe_2(SO_4)_3 \cdot nH_2O$ phase will form will be the activity of water in this liquid, and not the fugacity of the water vapor. The Pitzer model for $Fe_2(SO_4)_3$-rich solutions (Tosca et al. 2007) predicts that the activity of water in such solutions can be as low as 0.44. Hence, if rhomboclase is present in these samples, they cannot be used as temperature-RH brackets anymore. Currently, other groups (Wang et al. 2008) are using different starting phases for the temperature-RH brackets and possibly solve the problems associated with the interfering rhomboclase.

(3) Combination of solubility data with the measured enthalpies of formation and entropy estimates. The recently published Pitzer model coefficients for the system $Fe_2(SO_4)_3$-H_2SO_4-H_2O (Tosca et al. 2007) would then allow for optimization of the existing thermodynamic data. However, no solubility data at room temperature exist for coquimbite or paracoquimbite, and kornelite and $Fe_2(SO_4)_3 \cdot 5H_2O$ are probably unstable at this temperature in contact with aqueous media. The existing solubility data for rhomboclase and ferricopiapite (Cameron and Robinson 1907; Posnjak and Merwin 1922; Baskerville and Cameron 1935), the thermodynamic data (Majzlan et al. 2006), and the Pitzer model appear to have some potential (see discussion in Tosca et al. 2007).

We are currently working along all of these directions and each of them presents their own unique set of challenges. Additional challenges in this system are the variable hydration state of kornelite, the possibility that coquimbite and paracoquimbite are not true polymorphs, and the variable structures of the copiapite-group minerals (Majzlan and Michallik 2007). Nevertheless, once at least some of the problems are solved, we will be able to calculate phase diagrams for the ferric sulfates and predict their dissolution-crystallization behavior in nature. All the data sources can then be combined to produce an internally consistent data set for the AMD minerals, a data set that is largely nonexistent today.

ACKNOWLEDGMENTS

We thank J.A. Hurowitz and an anonymous reviewer for thoughtful comments and D. Dyar for the editorial handling of the manuscript. We are grateful to N. Tosca for the fruitful discussions of the Pitzer model, M. Schrage for the preparation of the kornelite thin sections, and H. Müller-Sigmund for help with electron microprobe analyses. We acknowledge the Angströmquelle Karlsruhe (ANKA) (Forschungszentrum Karlsruhe, Germany) for the provision of the beamtime. This study was financially supported by a Deutsche Forschungsgemeinschaft grant no. MA3927/2-1.

REFERENCES CITED

Balistrieri, L.S., Seal II, R.R., Piatak, N.M., and Paul, B. (2007) Assessing the concentration, speciation, and toxicity of dissolved metals during mixing of acid-mine drainage and ambient river water downstream of the Elizabeth Copper Mine, Vermont, U.S.A. Applied Geochemistry, 22, 930–952.

Baron, D. and Palmer, C.D. (2002) Solid-solution aqueous-solution reactions between jarosite $[KFe_3(SO_4)_2(OH)_6]$ and its chromate analog. Geochimica et Cosmochimica Acta, 66, 2841–2853.

Baskerville, W.H. and Cameron, F.H. (1935) Ferric oxide and aqueous sulfuric acid at 25 °C. Journal of Physical Chemistry, 39, 769–779.

Bridges, J.C. and Grady, M.M. (2000) Evaporite mineral assemblages in the nakhlite (martian) meteorites. Earth and Planetary Science Letters, 176, 267–279.

Cameron, F.K. and Robinson, C. (1907) Ferric sulphates. Journal of Physical Chemistry, 11, 641–650.

Chipera, S.J., Vaniman, D.T., and Bish, D.L. (2007) The effect of temperature and water on ferric-sulfates. Lunar and Planetary Science Conference, XXXVIII, abstract 1409.

DeKock, C.W. (1986) Thermodynamic properties of selected metal sulfates and their hydrates, 59 p. U.S. Bureau of Mines, Information Circular, 9081.

Giester, G. and Miletich, R. (1995) Crystal structure and thermal decomposition of the coquimbite-type compound $Fe_2(SeO_4)_3 \cdot 9H_2O$. Neues Jahrbuch für Mineralogie, Monatshefte, 5, 211–223.

Hasenmueller, E.A. and Bish, D.L. (2005) The hydration and dehydration of ferric iron sulfates. Lunar and Planetary Science Conference, XXXVI, abstract 1164.

Hemingway, B.S., Seal II, R.R., and Chou, I.M. (2002) Thermodynamic data for modeling acid mine drainage problems: Compilation and estimation of data for selected soluble iron-sulfate minerals, 13 p. U.S. Geological Survey, Open File Report, 02-161.

Holland, T.J.B. (1989) Dependence of entropy on volume for silicate and oxide minerals: A review and predictive model. American Mineralogist, 74, 5–13.

Jambor, J.L., Nordstrom, K.D., and Alpers, C.N. (2000) Metal-sulfate salts from sulfide mineral oxidation. In C.N. Alpers, J.L. Jambor, and D.K. Nordstrom, Eds., Sulfate Minerals—Crystallography, Geochemistry, and Environmental Significance, 40, p. 304–350. Reviews in Mineralogy and Geochemistry, Mineralogical Society of America, Chantilly, Virginia.

Joeckel, R.M., Ang Clement, B.J., and VanFleet Bates, L.R. (2005) Sulfate-mineral crusts from pyrite weathering and acid rock drainage in the Dakota Formation and Graneros Shale, Jefferson County, Nebraska. Chemical Geology, 215, 433–452.

Johnson, R.D., Bell, J.F., Cloutis, E., Staid, M., Farrand, W.H., McCoy, T., Rice, M., Wang, A., and Yen, A. (2007) Mineralogic constraints on sulfur-rich soils from Pancam spectra at Gusev crater, Mars. Geophysical Research Letters, 34, L13202.

Larson, A.C. and Von Dreele, R.B. (1994) General structure analysis system (GSAS). Los Alamos National Laboratory Report LAUR 86-748.

Latimer, W.L. (1952) Oxidation Potentials, 92 p. Prentice Hall, New York.

Majzlan, J. and Michallik, R. (2007) The crystal structures, solid solutions and infrared spectra of copiapite-group minerals. Mineralogical Magazine, 71, 557–573.

Majzlan, J., Grevel, K.-D., and Navrotsky, A. (2003) Thermodynamics of iron oxides: Part II. Enthalpies of formation and relative stability of goethite (α-FeOOH), lepidocrocite (γ-FeOOH), and maghemite (γ-Fe_2O_3). American Mineralogist, 88, 855–859.

Majzlan, J., Stevens, R., Donaldson, M., Boerio-Goates, J., Woodfield, B.F., and Navrotsky, A. (2005) Thermodynamics of monoclinic $Fe_2(SO_4)_3$. Journal of Chemical Thermodynamics, 37, 802–809.

Majzlan, J., Navrotsky, A., McCleskey, R.B., and Alpers, C.N. (2006) Thermodynamic properties and crystal structure refinement of ferricopiapite, coquimbite, rhomboclase, and $Fe_2(SO_4)_3(H_2O)_5$. European Journal of Mineralogy, 18, 175–186.

Marriott, R.A., Stancescu, M., Kennedy, C.A., and White, M.A. (2006) Technique for determination of accurate heat capacities of volatile, powdered, or air-sensitive samples using relaxation calorimetry. Review of Scientific Instruments, 77, 096108.

Merwin, H.E. and Posnjak, E. (1937) Sulfate incrustations in the copper queen mine, Bisbee, Arizona. American Mineralogist, 22, 567–571.

Morris, R.V., Klingelhofer, G., Schroder, C., Rodionov, D.S., Yen, A., Ming, D.W., de Souza, P.A., Wdowiak, T., Fleischer, I., Gellert, R., Bernhardt, B., Bonnes, U., Cohen, B.A., Evlanov, E.N., Foh, J., Gutlich, P., Kankeleit, E., McCoy, T., Mittlefehldt, D.W., Renz, F., Schmidt, M.E., Zubkov, B., Squyres, S.W., and Arvidson, R.E. (2006) Mössbauer mineralogy of rock, soil, and dust at Meridiani Planum, Mars: Opportunity's journey across sulfate-rich outcrop, basaltic sand and dust, and hematite lag deposits. Journal of Geological Research: Planets, 111, E12S15.

Nordstrom, D.K. and Alpers, C.N. (1999) Negative pH, efflorescent mineralogy, and consequences for environmental restoration at the Iron Mountain Superfund site, California. Proceedings of the National Academy of Sciences, 96, 3455–3462.

Pankratz, L.B. and Weller, W.W. (1969) Thermodynamic data for ferric sulfate and indium sulfate. U.S. Bureau of Mines, Report of Investigations, 7280.

Parker, V.B. (1965) Thermal properties of uni-univalent electrolytes. National Standard Reference Data Series, National Bureau of Standards, 2, 66 p.

Pitzer, K.S. and Coulter, L.V. (1938) The heat capacities, entropies, and heats of solution of anhydrous sodium sulfate and of sodium sulfate decahydrate. The application of the third law of thermodynamics to hydrated crystals. Journal of the American Chemical Society, 60, 1310–1313.

Posnjak, E. and Merwin, H.E. (1922) The system, Fe_2O_3-SO_3-H_2O. Journal of the American Chemical Society, 44, 1965–1994.

Qin, K.Z., Ding, K.S., Xu, Y.X., Miao, Y., Fang, T.H., and Xu, X.W. (2008) Tremendous crystal-paracoquimbite and its polytype coquimbite found for the first time in Hongshan Hs-epithermal Cu-Au deposit, eastern Tianshan, NW-China, and its significance. Acta Petrologica Sinica, 24, 1112–1122.

Quartieri, S., Sani, A., Vezzalini, G., Galli, E., Fois, E., Gamba, A., and Tabacchi, G. (1999) One-dimensional ice in bikitaite: single-crystal X-ray diffraction, infra-red spectroscopy, and ab-initio molecular dynamics studies. Microporous and Mesoporous Materials, 30, 77–87.

Robie, R.A. and Hemingway, B.S. (1995) Thermodynamic properties of minerals and related substances at 298.15 K and 1 bar (10^5 Pascals) and at higher temperatures. U.S. Geological Survey Bulletin, 2131, 461 p.

Robinson, P.D. and Fang, J.H. (1971) Crystal structures and mineral chemistry of hydrated ferric sulfates: II. The crystal structure of paracoquimbite. American Mineralogist, 56, 1567–1572.

——— (1973) Crystal structures and mineral chemistry of hydrated ferric sulfates. III. The crystal structure of kornelite. American Mineralogist, 58, 535–539.

Ruben, H.W., Templeton, D.H., Rosenstein, R.D., and Olovsson, I. (1961) Crystal structure and entropy of sodium sulfate decahydrate. Journal of the American Chemical Society, 83, 820–824.

Taylor, J.R. (1982) An Introduction to Error Analysis. The Study of Uncertainties in Physical Measurements, 70 p. Oxford University Press, U.K.

Tosca, N.J., Smirnov, A., and McLennan, S.M. (2007) Application of the Pitzer ion interaction model to isopiestic data for the $Fe_2(SO_4)_3$-H_2SO_4-H_2O system at 298.15 and 323.15 K. Geochimica et Cosmochimica Acta, 71, 2680–2698.

Van Nuys, C.C. (1943) Enthalpy and heats of dilution of the system HCl-H_2O. Transactions of the American Institute of Chemical Engineers, 39, 663–678.

Wang, A., Ling, Z., and Freeman, J.J. (2008) Ferric sulfates on Mars: Surface explorations and laboratory experiments. EOS Transactions AGU 89, Fall Meeting Supplement, abstract P44A-08.

MANUSCRIPT RECEIVED DECEMBER 22, 2008
MANUSCRIPT ACCEPTED JULY 20, 2009
MANUSCRIPT HANDLED BY M. DARBY DYAR